

2

**AD-A253 289**

PL-TR-92-2024



**COMPOSITION OF SHORT PERIOD REGIONAL  
PHASES INFERRED FROM FENNOSCANDIAN ARRAY DATA**

Kristín S. Vogfjörð  
Charles A. Langston  
Ben Yan

Pennsylvania State University  
114 Kern Building  
University Park, PA 16802

31 December 1991

Scientific Report No. 1

**DTIC**  
**SELECTE**  
**JUN 23 1992**  
**S B D**

Approved for public release; distribution unlimited.




**PHILIPS LABORATORY**  
**AIR FORCE SYSTEMS COMMAND**  
**HANSCOMB AIR FORCE BASE, MASSACHUSETTS 01731-5000**


92 6 22 013

**92-16376**

The views and conclusions contained in this document are those of the authors and should not be interpreted as representing the official policies, either expressed or implied, of the Air Force or the U.S. Government.

This technical report has been reviewed and is approved for publication.

  
JAMES F. LEWKOWICZ  
Contract Manager  
Solid Earth Geophysics Branch  
Earth Sciences Division

  
JAMES F. LEWKOWICZ  
Branch Chief  
Solid Earth Geophysics Branch  
Earth Sciences Division

  
DONALD H. ECKHARDT, Director  
Earth Sciences Division

This document has been reviewed by the ESD Public Affairs Office (PA) and is releasable to the National Technical Information Service (NTIS).

Qualified requestors may obtain additional copies from the Defense Technical Information Center. All others should apply to the National Technical Information Service.

If your address has changed, or if you wish to be removed from the mailing list, or if the addressee is no longer employed by your organization, please notify PL/IMA, Hanscom AFB MA 01731-5000. This will assist us in maintaining a current mailing list.

Do not return copies of this report unless contractual obligations or notices on a specific document requires that it be returned.

REPORT DOCUMENTATION PAGE			Form Approved OMB No. 0704-0188	
Public reporting burden for this collection of information is estimated to average 1 hour per response, including the time for reviewing instructions, searching existing data sources, gathering and maintaining the data needed, and completing and reviewing the collection of information. Send comments regarding this burden estimate or any other aspect of this collection of information, including suggestions for reducing this burden, to Washington Headquarters Services, Directorate for Information Operations and Reports, 1215 Jefferson Davis Highway, Suite 1204, Arlington, VA 22202-4302, and to the Office of Management and Budget, Paperwork Reduction Project (0704-0188), Washington, DC 20503.				
1. AGENCY USE ONLY (Leave blank)	2. REPORT DATE 31 December 1991	3. REPORT TYPE AND DATES COVERED Scientific No. 1		
4. TITLE AND SUBTITLE Composition of Short-Period Regional Phases Inferred From Fennoscandian Array Data		5. FUNDING NUMBERS PE 62101F PR 7600 TA 09 WU AQ Contract F19628-90-K-0044		
6. AUTHOR(S) Kristin Vogfjord Charles A. Langston Ben Yan				
7. PERFORMING ORGANIZATION NAME(S) AND ADDRESS(ES) Pennsylvania State University 114 Kern Building University Park, PA 16802		8. PERFORMING ORGANIZATION REPORT NUMBER		
9. SPONSORING/MONITORING AGENCY NAME(S) AND ADDRESS(ES) Phillips Laboratory Hanscom AFB, MA 01731-5000  Contract Manager: James Lewkowicz/GPEH		10. SPONSORING/MONITORING AGENCY REPORT NUMBER  PL-TR-92-2024		
11. SUPPLEMENTARY NOTES				
12a. DISTRIBUTION/AVAILABILITY STATEMENT  Approved for public release; Distribution unlimited			12b. DISTRIBUTION CODE	
13. ABSTRACT (Maximum 200 words) Short-period seismograms from local and regional events recorded at the NORESS and ARCESS arrays are being studied in order to understand the composition of local and regional phases and to separate the effects of structure & source parameters on the seismic signal. This is a precondition for accurate phase identification and accordingly, for reliable location of events within regional distances. f-k analysis is used to identify and locate arrivals in the seismograms and a composite of array beams is used as an approximation to each event. Inferences about structure differences at ARCESS and NORESS are made by comparing composite-seismogram record sections from the two sites. Synthetic P-wave seismograms are calculated for velocity models representing the average structure of the propagation paths. The effects of near-receiver and source structure on regional phases, need to be understood and separated from the effects of propagation path. For this purpose receiver functions obtained from teleseismic events, recorded at the three-component, intermediate-period channels, EO at NORESS and ARCESS are being analyzed. Average Moho depth of 35 km is obtained under NORESS by stacking receiver functions from all events. The effects of a surface scatterer at Lake Mjosa are seen in one event.				
14. SUBJECT TERMS ARCESS                      Regional wave propagation NORESS                     Receiver functions			15. NUMBER OF PAGES 40	
			16. PRICE CODE	
17. SECURITY CLASSIFICATION OF REPORT Unclassified	18. SECURITY CLASSIFICATION OF THIS PAGE Unclassified	19. SECURITY CLASSIFICATION OF ABSTRACT Unclassified	20. LIMITATION OF ABSTRACT SAR	

## Table of Contents

List of Scientist Contributing to this Report	iv
List of Previous Contracts Related to this Research	iv
Report Summary	iv
Task Objectives	iv
Technical Problem	iv
General Methodology	v
Technical Results	v
Important Findings and Conclusions	vi
Significant Hardware Development	vi
Special Comments	vi
Introduction	1
Research Accomplished:	4
Regional Phases at ARCESS	4
Receiver Functions at NORESS	8
Conclusions and Future Plans	9
References	10



<b>Accession For</b>	
NTIS GRA&I	<input checked="" type="checkbox"/>
DTIC TAB	<input type="checkbox"/>
Unannounced	<input type="checkbox"/>
Justification	
By	
Distribution/	
Availability Codes	
Dist	Avail and/or Special
A-1	

## **List of Scientist Contributing to this Report**

Charles A. Langston , P.I.  
Kristín Vogfjörð, Research Assistant  
Ben Yan, Research Assistant

## **List of Previous Contracts Related to this Research**

Wave Propagation at Regional Distances, Contract # F19628-89-K-0013

## **Report Summary**

### **Task Objectives**

Characterization of local and regional wave propagation in the crust and upper mantle around the three short-period Fennoscandian arrays, NORESS, ARCESS and FINESA.

### **Technical Problem**

Short-period, small-aperture arrays are key to reliable regional nuclear test monitoring. The array geometries enable phase detection at small amplitudes and allow determination of backazimuth and phase velocity. Assuming a velocity model, event distance can then be deduced from relative arrival times and phase velocities of major phases. In order to obtain accurate source distances and avoid misidentifying phases or missing small arrivals in events, it is therefore necessary to know the local and regional velocity structure and its effect on wave propagation near the arrays.

Previous work on events at local distances from the NORESS array has shown that mislocations occur due to missed small amplitude  $P_n$  arrivals and misidentified onset of  $L_g$ . Furthermore, earthquakes at local distances from NORESS do not produce depth phases of significant amplitudes, making source-depth discrimination dependent on the existence of accurate travel-time curves for near-surface sources. The present work focuses on studying regional wave propagation near ARCESS, and in addition the

effects of receiver structure at NORESS and ARCESS. Behavior of the main regional phases with distance and azimuth is studied in ARCESS data from regional events. Receiver structure under NORESS is studied through receiver function analysis of teleseismic events recorded at the three-component intermediate-period elements, NRE0.

### **General Methodology**

Regional phases are studied through array-analysis.  $f$ - $k$  analysis is applied in sliding time windows to detect phases and determine phase velocities and azimuth of approach. Composite seismograms for the events are made from time pieces of array beams, with each time section representing an arrival. Composite-seismogram record sections are constructed and compared to synthetic-seismogram record sections, calculated by wavenumber integration in plane-layered constant-velocity models.

Receiver structure is studied through receiver function analysis of teleseismic events. Receiver functions are calculated for all events and stacked to lower the effects of noise. Synthetic receiver functions are then calculated for different velocity models and matched, by trial and error, to the stack of observed receiver functions.

### **Technical Results**

Mislocations with the Intelligent Monitoring System of small events around ARCESS are mainly due to misidentified onset of  $L_g$ ; multipathing also causes some azimuthal uncertainties. Mislocations due to missed  $P_n$  arrivals are not observed, since  $P_n$  amplitudes are relatively large. Lateral velocity variations appear to be associated with the Lapland Granulite region and the Polmak-Pasvik-Pechenga belt, causing apparent multipathing and phase velocity variations. Crustal thickness around ARCESS varies between 42 and 45 km.

Characteristic of the seismic record section from ARCESS is the absence of multiple crustal arrivals at any distance. This can be explained by a velocity gradient above the Moho, causing the energy of each reverberation and

multiples to be concentrated over a small distance interval.  $R_g$  is observed out to at least 400 km distance.

Crustal thickness under NORESS is 35 km and may be shallower towards the Oslo Graben. No large crustal discontinuities are detected with receiver function analysis. Apparent secondary  $R_g$  waves seem to stem from the surface Topography at Lake Mjøsa.

### **Important Findings and Conclusions**

Significant lateral velocity variations affect the wave propagation in the ARCESS region. Higher velocity gradients above and below the Moho and a thicker crust also result in different record sections at ARCESS from those at NORESS: At NORESS, a low velocity gradient above the Moho results in multiple crustal reverberations observed at any distance, and a low velocity gradient below the Moho causes small  $P_n$  waves. At ARCESS, on the other hand, the high gradients produce larger  $P_n$  waves and focus the energy of each crustal reverberation over a small distance interval. The low relief in the ARCESS region also allows more efficient propagation of  $R_g$ .

Due to the discrete nature of arrivals in the array seismograms, the characteristics of the record section at ARCESS, as well as at NORESS can be explained in terms of plane-layered velocity models. Although actual velocity and thickness variations cause the observed record sections to deviate from these simple models, the models enable reliable identification of the various phases observed and thus result in more accurate locations.

### **Significant Hardware Development**

N/A

### **Special Comments**

N/A

## **Introduction**

Short-period seismograms from events at local and regional distances consist of a multitude of complex arrivals mixed in with incoherent scattered energy and noise. For source distances well into the regional range however, the seismograms are commonly dominated by discrete arrivals with distinct phase velocities. Timing, amplitude and phase velocities of these dominant phases are controlled by crustal and upper mantle structure as well as source parameters. In order to properly identify the arrivals and thus obtain reliable locations for the events, average structure along the propagation paths must first be obtained. When amplitude and travel-time behavior of the major phases with distance is known for all azimuth directions, it becomes possible to distinguish near-source surface reflections, or depth phases, from the train of arrivals in a regional seismogram. Depth phases reveal source depth, which for discriminatory purposes is the most important source parameter.

Array data allows the association of phase velocities with individual arrivals. This makes phase identification more reliable and enables tracing arrivals over distance. From the travel-time curves obtained, the gross structure may then be deduced. Due to the discrete nature of the arrivals and the domination of coherent phases over incoherent scattered energy, a central-element seismogram can in most cases be approximated by a composite of array beams, with each time section of a beam representing an arrival. This has been demonstrated for several events recorded at NORESS (Vogfjörd and Langston, 1991). The composite seismogram enhances coherent arrivals, while incoherent energy and noise are diminished. The difference between a composite seismogram and the original data gives an estimate of the incoherent, scattered energy caused by structural heterogeneities and determines the appropriateness of modeling with plane-layered, isotropic velocity structure.

Results from the short-period regional data can be augmented by receiver function analysis of teleseismic events recorded at the three-component elements of the arrays. In particular, the velocity function under a recording site can be studied independent of path propagation, allowing velocity contrasts such as the crust-mantle interface to be located. Knowing the near-array structure, the site response can then be modeled



and separated from the regional path effects. The receiver-function method entails deconvolving the vertical component of motion in the teleseismic P-wave window from the radial component. This removes the effects of source time function and source structure, as well as the effects of instrument response and propagation through the mantle. What is then left on the deconvolved radial component are the P-to-S (Ps) conversions occurring at velocity discontinuities under the receiver. Descriptions of the receiver-function method are given by Langston (1979) and Owens et al. (1987).

The crustal and upper mantle structure around the NORESS and ARCESS arrays has been extensively studied with refraction surveys. The structure around NORESS is defined by three geological provinces: The Precambrian crust of the southern Baltic Shield, the Oslo Graben within the Precambrian region and the Caledonian fold chain, which extends along the entire west coast of Scandinavia (Figure 1). Velocity models for the Graben and the Precambrian region east of the Graben were obtained from a study of local events recorded at NORSAR (Gundem, 1984). Several different velocity models have been obtained for the Caledonian region (Kanestrøm and Haugland, 1971; Sellevoll and Warrick, 1971; Mykkeltveit, 1980). The Caledonian model used here is a combination of an upper crust from the Precambrian model and a lower crust similar to the models obtained from the Årsund-Otta (Mykkeltveit, 1980) and the 3-4 (Kanestrøm and Haugland, 1971) profiles (Figure 1). NORESS is located in the Precambrian region and therefore the Precambrian model is used in the receiver function modeling. The local and regional events presented from NORESS are all, except one, located in the Caledonides with propagation paths mostly within the region. The travel-time curves and synthetic seismograms calculated for the NORESS region are therefore based on the Caledonian model. The two models are shown in Figure 2a and 2b.

ARCESS is located in the oldest, Archaean, part of the Baltic Shield (Figure 3), just west of the Proterozoic, Lapland Granulite Belt. The granulite belt is a wedge-shaped body, believed to be a slice of continental crust overthrust on to the Archaean basement to the south in a continent-continent collision during the Proterozoic. The suture zone between these colliding continents is along the Polmak-Pasvik-Pechenga Belt, which

consists of Proterozoic volcanic rocks and runs approximately NW-SE along the Kola peninsula (Gaál et al, 1989). The PPP Belt has been penetrated by the Kola superdeep drillhole (Figure 3). The velocity profile in the drillhole is reversed, with highest velocities in the upper 6.8 km, which constitute the Proterozoic section. Below that the Archaean basement is reached (Kozlovsky, 1987).

Several refraction profiles cross the region: The northernmost section of the Fennolora profile runs just west of ARCESS (Galson and Mueller, 1986; Guggisberg et al., 1991; Lund, 1987) and the Polar profile, crosses the Granulite belt and the suture zone east of ARCESS (Luosto et al., 1989) (Figure 3). The Polar profile also has a reflection section where the profile crosses the Lapland Granulite Belt (Behrens et al., 1989). Kola Peninsula has been explored on several refraction profiles (Azbel et al., 1989; Glaznev et al., 1989) and the area south of the array is sampled by the Finlap profile (Luosto et al, 1983). One- (Lund, 1987) and two-dimensional (Guggisberg et al., 1991) velocity interpretation of the northern section of Fennolora includes low-velocity zones in the upper crust of the Caledonian region and a 45 km thick crust. 2-D modeling of the Polar profile reveals a NW dipping high-velocity layer coinciding with the Granulite belt, and an undulating Moho, with the thinnest crust in the middle of the profile. 2-D interpretation of the Kola Peninsula profiles requires an approximately 40 km wide and 10 km deep high-velocity gradient zone in the approximate location of the Granulite belt and an undulating Moho (Azbel et al., 1989). Moho depths increase from 36 km, under northeastern Kola Peninsula, to 44 km under the southwestern Peninsula. One-dimensional modeling of Finlap includes a 50 km thick crust (Luosto et al., 1983).

Locations of the events selected are shown in Figure 3. All events west of ARCESS are within the Archaean region, with partial travel-paths through the Granulite belt, and most events on the Kola peninsula are located near the PPP zone. Other events are in the younger, Proterozoic region south of the array, and one is in the Caledonian region, which extends along the western coast. The velocity model used here, in travel-time and synthetic seismogram calculations is a plane-layered approximation to the northern section of the Polar profile and is shown in Figure 2c.

In a previous study local and regional events recorded at NORESS were analyzed (Vogfjörð, 1991). In the present study the research is focussed on regional ARCESS data. Arrivals in the seismograms are detected and identified with f-k analysis in sliding time windows, beams are formed for the major phases, and time sections of the beams then pieced together to form the composite seismogram for each event. A seismic record sections of composite seismograms from ARCESS is constructed and compared to a record section from NORESS, and behavior of the dominating phases with distance is examined. The composite record sections reveal the behavior of relative amplitudes and travel times with distance, thus allowing conclusions about crustal and upper mantle structure to be drawn. Synthetic P-wave record sections calculated for plane-layered isotropic models are also presented in an attempt to explain the apparent differences between the two regions.

Receiver functions from teleseismic events recorded on the three-component, intermediate-period channels E0, at the center of NORESS and ARCESS are being analyzed. Results from NORESS are presented and the Ps conversion at the Moho is modeled. Crustal discontinuities are not resolved, but a surface scatterer is identified, producing strong coda waves.

## Research Accomplished:

### *Regional Phases at ARCESS*

Twenty two seismic events at local and regional distances from ARCESS were selected from the IMS bulletin at CSS. The events cover a distance range of 175 to 575 km and local magnitude range ( $M_l$ ) is from 2.0 to 3.2. Most locations coincide with known mines and are therefore likely mine explosions. A study of eight events has already been completed. Event locations are shown in Figure 3. Due to misidentified onset of  $L_g$ , two events are mislocated by the Intelligent Monitoring System, by approximately 30 km. In event 167198 at 175 km distance,  $S_g$  is the first arrival followed by a larger  $S_mS$  phase (Figure 4), which is mistakenly picked as the first S-arrival. In event 335253 at 220 km distance  $S_mS$  is missed and the following larger phase,  $2 \times S_mS$ , is picked as the onset of  $L_g$ . Events due east from ARCESS show a significant amount

of variation in backazimuth within each phase. This variation, which is probably due to lateral multipathing may be causing a mislocation of up to  $10^\circ$  in event 326360 at 200 km distance.

Composite-seismogram record sections of the events completed are shown in Figure 4a and b, with stacking velocities indicated above each beam section. Event 348962 has been high-pass filtered at 1.5 Hz to reduce low-frequency noise. The travel-time curves shown, were calculated for a plane-layered approximation to the Polar-Profile model (Luosto et al., 1989) with a crustal thickness of 42 km. The move-out of the dominant phases approximately follow the travel-time curves, indicating an adequate velocity model. Lack of events within 175 km from the array, however, precludes resolution of detailed crustal structure and the observed deviations of the Moho reflections from the travel-time curves also indicates variations in crustal thickness.

The main characteristics of the record section in Figure 4a are apparent discrete arrivals, each mostly dominated by a single phase velocity. In event 240323, at 575 km distance, the phase velocities obtained in the  $L_g$  wave train however are more varied, although the wave train is dominated by 3.0 km/s and 4.6 km/s waves. Relatively large upper mantle waves,  $P_n$  and  $S_n$ , are also observed, probably caused by a considerable velocity gradient just below the Moho.  $P_g$  is the first arrival in event 167198 at 175 km distance, at 200 km  $P_g$ ,  $P_mP$  and  $P_n$  arrive approximately simultaneously, and beyond that  $P_n$  is the first arrival. The relative arrival times of the inferred  $P_g$  and  $P_mP$  phases in the event at 175 km distance, as compared to the travel-time curves, may indicate a deeper Moho at 90 km distance east of the array. However, it could also be caused by a ripple fired explosion, in which case both P arrivals are interfering  $P_g$  and  $P_mP$ . Event 348962 also appears to be near the crossover distance for  $P_n$ ,  $P_mP$  and  $P_g$  indicating a deeper Moho than 42 km.

The first Moho reflections ( $P_mP/S_mS$ ) dominate the seismograms out to approximately 300 km distance. Beyond that distance the second crustal reverberations take over, while the first ones disappear. The upper mantle waves experience increase of amplitude with distance so that in event 240323, at 575 km distance they dominate. A clear double arrival is observed in the  $P_n$  wave train at 575 km distance followed by a third, 9.1 km/s arrival, possibly  $2 \times P_n$ . Whether the second arrival is a source or a

structure effect will be determined by examining other events from this location. Only in event 335253, at 350 km distance are there more than one Moho reverberation observed, i.e.  $S_mS$  and  $2 \times S_mS$ . This absence of multiples can be explained by a strong velocity gradient in the lower crust, causing focussing of the energy of each crustal reverberation over a short distance interval. This is consistent with the Polar-Profile model (Luosto et al., 1989).

$R_g$  is observed out to 400 km distance, and moves out with a group velocity of 2.9 km/s. The interference apparent in  $R_g$  of events 167198 at  $86.0^\circ$  backazimuth and event 326360 at  $95.5^\circ$  backazimuth, is not observed in  $R_g$  of event 282554 (Figure 4b), which is at approximately the same location as event 326320 and is also much larger than the other two. This difference therefore is probably a source effect - such as a ripple-fired explosion - rather than a structure effect, although the location of the events in and around the PPP Belt may cause multipathing near the surface.

Event 392876 is located in the Precambrian region southwest of ARCESS. The propagation path is along the eastern margin of the Caledonian region and crosses a section of the Fennolora profile which has complex upper crustal structure (Lund, 1987; Guggisberg et al., 1991). This may be the cause of the small amplitude  $P_n$  and the apparent multiple crustal arrivals observed in the P wave train. The multiple arrivals however, could be due to source time function and/or source depth.  $R_g$  was not detected in the unfiltered records, but due to the low amplitudes, may have been buried in the low-frequency noise. The apparent absence of  $R_g$  could be the result of considerable source depth, but the location of the event near Kiruna, suggests an explosion source. Analysis of more events from this location is necessary to distinguish structure and source effects.

The record section in Figure 4a shows a distinctly different character from record sections of composite seismograms from the NORESS array. For comparison, a record section of seven events from a previous study (Vogfjörð, 1991), with locations as shown in Figure 1 is plotted in Figure 5. Travel-time curves calculated for a Caledonian model, 36-km thick, are superimposed on the record section. All events, except one, B-5, are located within the Caledonides, with propagation paths mainly within Caledonian structure. The record section reveals small upper mantle waves, more than one Moho reverberation in events from

distances beyond approximately 200 km, and inefficient propagation of  $R_g$  waves within the Caledonides. The small upper-mantle waves are caused by a small or no velocity gradient below the Moho. The occurrence of large double reverberations ( $2 \times P_m P$  and  $2 \times S_m S$ ), while the first reflections ( $P_m P$  and  $S_m S$ ) still remain large can be explained by gradual velocity increase in the upper to intermediate crust and a near-constant velocity in the lower crust. Due to scattering by surface topography in the Caledonides,  $R_g$  does not propagate to 200 km distance. Propagation through Precambrian structure is more efficient, as can be seen in event B-5, which has an  $R_g$  wave of significant amplitude. The model used for travel-time calculations represents average structure in the Caledonides: a plane-layered 36 km thick crust, with a gradual velocity increase in the intermediate crust and constant velocity in the lower crust (Vogfjörð, 1991).

To illustrate the difference between the Caledonian and the Polar-profile velocity models, synthetic seismograms are calculated by wavenumber integration in plane-layered constant-velocity models, which are approximations to the gradient models. The P-wave velocity models are plotted in Figure 2b and c. To facilitate the comparison, the thickness of the bottom crustal layer in the Caledonian model is increased to make crustal thickness equal that of the Polar-profile model. Integration is performed over ray parameters from 0.01 to 0.2 s/km; including only P-waves. The source time function used is triangular, of 0.1 s duration and sampling frequency is 10 Hz. The synthetic record sections together with travel-time curves are plotted in Figures 6 and 7. The synthetic Polar-Profile record section, in Figure 6, shows large amplitude  $P_n$  waves and concentration of the energy in each Moho reverberation over a distance interval of roughly 200 km. This is in general accordance with the composite record section in Figure 3a. The Caledonian-model record section in Figure 7, on the other hand, has small  $P_n$  waves and two to three Moho reverberations of significant amplitude at each distance beyond the critical distance for  $2 \times P_m P$ . Due to the gradual increase in velocity throughout the intermediate crust, only the Moho reflections show up as discrete impulsive arrivals.

### ***Receiver Functions at NORESS***

21 teleseismic events recorded at NORESS were used to calculate receiver functions in order to obtain crustal thickness and velocity profile under the array. The events, listed in Table 1 are at epicentral distances of  $30^\circ$  to  $90^\circ$ , with  $M_b \geq 5.8$ . Azimuthal coverage is mostly in the northern quadrants. Event locations are shown in Figure 8. Due to noise in the data stacking was necessary to improve the signal-to-noise ratio. In the stacked data, the only observed Ps conversion occurs at the Moho. Using the Precambrian velocity model, synthetic receiver functions were calculated and fitted to the stacked receiver function. By trial and error, the best fit was obtained for a 35 km thick crust. In accordance with the stacked data, the synthetic receiver function produced by the Precambrian model has only one apparent Ps conversion, which occurs at the Moho. The discontinuities in the crust are too small to produce significant Ps conversions. The data and synthetic are shown in Figure 9a. Two individual events were of high enough quality to allow inspection of Moho depth variation with backazimuth. The receiver functions for these events and synthetic are shown in Figure 9b and c. For a backazimuth of  $336^\circ$ , the Moho depth is inferred 35 km, but for a backazimuth of  $262^\circ$ , a Moho depth of 33 km is deduced. Variations in crustal thickness around the NORESS array were indicated by previous studies (Berteussen, 1977, Gudem, 1984), with thickness decreasing under the Oslo Graben. This is consistent with the receiver-function results. Event 22, from  $75^\circ$  distance and  $38^\circ$  backazimuth has a high s/n ratio and large coda waves trailing the first P arrival by 10 seconds (Figure 10a). The particle motion in the propagation plane from the event is shown in Figure 10b for the 15-20 second time interval. If the horizontal components are rotated to  $45^\circ$  and  $135^\circ$ , as shown in Figure 11a, the coda wave is confined to the vertical and  $45^\circ$  components. The particle motion in the vertical- $45^\circ$  plane, shown in Figure 11b, is retrograde elliptical. The wave is therefore a secondary  $R_g$  wave caused by the surface topography, approximately 27 km SW of NORESS. This location coincides with lake Mjøsa.

## Conclusions and Future Plans:

Location of the ARCESS array just east of the Lapland Granulite belt appears to have an effect on the regional waveforms observed. Variations in backazimuth are considerable for events located near the Pechenga region and phase velocities in the  $L_g$  wavetrain from  $156^\circ$  backazimuth show considerable variation.

A significant difference is observed between the short-period seismograms recorded at NORESS and ARCESS, from local and regional events. The difference can be explained by a greater velocity gradient in the lower crust and upper mantle of northern Fennoscandia than in southern Norway. Furthermore, due to the lower relief in the area south and west of ARCESS, the  $R_g$  wave propagates to greater distances than in southern Norway. Mislocations by NORESS occur due to missed  $P_n$  arrivals and misidentified onset of  $L_g$  (Vogfjörd and Langston, 1991). At ARCESS,  $P_n$  is larger and therefore more easily detected. Consequently, mislocations by ARCESS are mainly due to misidentified  $L_g$  onset. The apparent multipathing from easterly azimuths may also be causing some azimuthal mislocation.

In the continuing study coverage at local distances around ARCESS is being improved. Up until recently only data at distances  $\geq 170$  km and of magnitude  $\geq 2.0$  were saved for the IMS database at CSS. Data from smaller distances are now available on-line in the IMS2 database. A scan of the parameter data indicates that coverage at local distances can be significantly improved. A few good- to high-quality local events have already been retrieved from IMS2. A more complete event coverage is expected to allow resolution of the crustal and upper mantle velocity profile around ARCESS. Modeling of  $R_g$  wave dispersion should also be possible with an increased number of local events.

Crustal thickness under NORESS as obtained by receiver-function analysis is 35 km, with indications of shallower (33 km) depths towards the Oslo Graben. The surface topography at Lake Mjøsa scatters the teleseismic P waves producing a large secondary  $R_g$  wave arriving approximately 10 seconds later than the P wave. The lake Mjøsa scatterer has been observed in previous teleseismic studies (Gupta et al., 1991,



Wagner and Langston, 1991) and apparent secondary  $R_g$  waves have also been observed from a local event (event D2 in Figure 1) with a propagation path across Lake Mjøsa (Vogfjörd, 1991).

Additional teleseismic data recorded at NORESS and ARCESS have been received from Norway and analysis of receiver functions at NORESS and ARCESS is now in progress.

The new IMS2 database also contains waveform data from the FINESA array in Finland. Analysis of local and regional events recorded by FINESA is the subject of future investigation in order to compare wave propagation through the Precambrian crust in Southern Finland to the Archaean crust of Lapland and the Precambrian and Caledonian crust of Southern Norway.

## References

- Azbel, I. Ya., A. F. Buyanov, V. T. Ionkis, N. V. Sharov and V. P. Sharova (1989). Crustal structure of the Kola Peninsula from inversion of deep seismic sounding data. *Tectonophysics*, **162**, 87-99.
- Behrens, K. S., S. Goldflam, P. Heikkinen, H. Hirschleber, G. Lindquist and C.-E. Lund (1989). Reflection seismic measurements across the Granulite Belt of the POLAR profile in the northern Baltic Shield, Northern Finland, *Tectonophysics*, **162**, 101-111.
- Berteussen, K. A. (1977). Moho depth determinations based on spectral-ratio analysis of NORSAR long-period P waves. *Phys. Earth Planet. Int.*, **15**, 13-27.
- Gaál, G., A. Berthelsen, R. Gorbatshev, R. Kesola, M. I. Lehtonen, M. Marker and P. Raase (1989). Structure and composition of the Precambrian crust along the Polar profile in the northern Baltic Shield, *Tectonophysics*, **162**, 1-25.
- Galson, G. A. and St. Mueller (1986). An introduction to the European Geotraverse Project: First results and present plans, *Tectonophysics*, **126**, 1-30.
- Glaznev, V. N., A. B. Raevsky and N. V. Sharov (1989). A model of the deep structure of the northeastern part of the Baltic Shield based on joint interpretation of seismic, gravity, magnetic and heat flow data, *Tectonophysics*, **162**, 151-163.
- Guggisberg, G., W. Kaminski and C. Prodehl (1991). Crustal structure of the Fennoscandian Shield: A travelttime interpretation of the long-range FENNOLORA seismic refraction profile, *Tectonophysics*, **195**, 105-137.
- Gundem, M. B. (1984). 2-D seismic synthesis of the Oslo Graben, *Cand. Scient. Thesis*, Inst of Geophysics, University of Oslo, Oslo, Norway, 164pp.
- Gupta, I. N., C. S. Lynnes, T. W. McElfresh and R. A. Wagner (1991). F-k analysis of NORESS array and single station data to identify sources of near-receiver and near-source scattering, *Bull. Seism. Soc. Am.*, **80**, 2227-2241.
- Kanestrøm, R. and K. Haugland (1971). Profile Section 3-4, in *Deep Seismic Sounding in Northern Europe*, A. Vogel, Editor, Swedish Natural Science Research Council, Stockholm, Sweden, 76-91.
- Kozlovsky, Ye. A. (Editor) (1987). *The Superdeep Well of the Kola Peninsula*, Springer-Verlag, Berlin, W-Germany, 558 pp.
- Langston, C. A. (1979). Structure under Mount Rainier, Washington, inferred from teleseismic body waves. *J. Geophys. Res.*, **84**, 4749-4762.

- Lund, C.-E. (1987). Crustal structure along the northern 'FENNOLORA' profile, *Precambrian Research*, **35**, 195-206.
- Luosto, U., S. M. Zverev, I. P. Kosminskaya, H. Korhonen (1983). Observations of Fennolora shots on additional line in Finnish Lapland. In: E. Bisztricsany and G. Szeidovitz (editors), *Proceedings of the 17th Assembly of the European Seismological Commission, Budapest, 1980*. Elsevier, Amsterdam, pp. 517-521.
- Luosto, U., E. R. Flueh, C.-E. Lund and Working Group (1989). The crustal structure along the POLAR profile from seismic refraction investigations, *Tectonophysics*, **162**, 51-85.
- Mykkeltveit, S. (1980). A seismic profile in Southern Norway, *Pure Appl. Geophys*, **118**, 1310-1325.
- Owens, T. J., S. R. Taylor and G. Zandt (1987). Crustal structure at regional test network stations determined from inversion of broadband teleseismic P wave forms, *Bull. Seism. Soc. Am.*, **77**, 631-662.
- Sellevoll, M. A. and R. E. Warrick, (1971). Refraction study of the crustal structure in southern Norway, *Bull. Seism. Soc. Am.*, **61**, 457-471.
- Vogfjörd, K. S., 1991. A study of NORESS-array seismograms from local and regional events, *Ph. D. Thesis*, Pennsylvania State University, University Park, 160 pp.
- Vogfjörd, K. S. and C. A. Langston (1991). Analysis of regional events recorded at NORESS, *Bull. Seism. Soc. Am.*, **80**, 2016-2031.
- Wagner, G. and C. A. Langston (1991). Body-to-surface wave scattered energy in teleseismic coda observed at the NORESS seismic array, *Bull. Seism. Soc. Am.*, **80**.

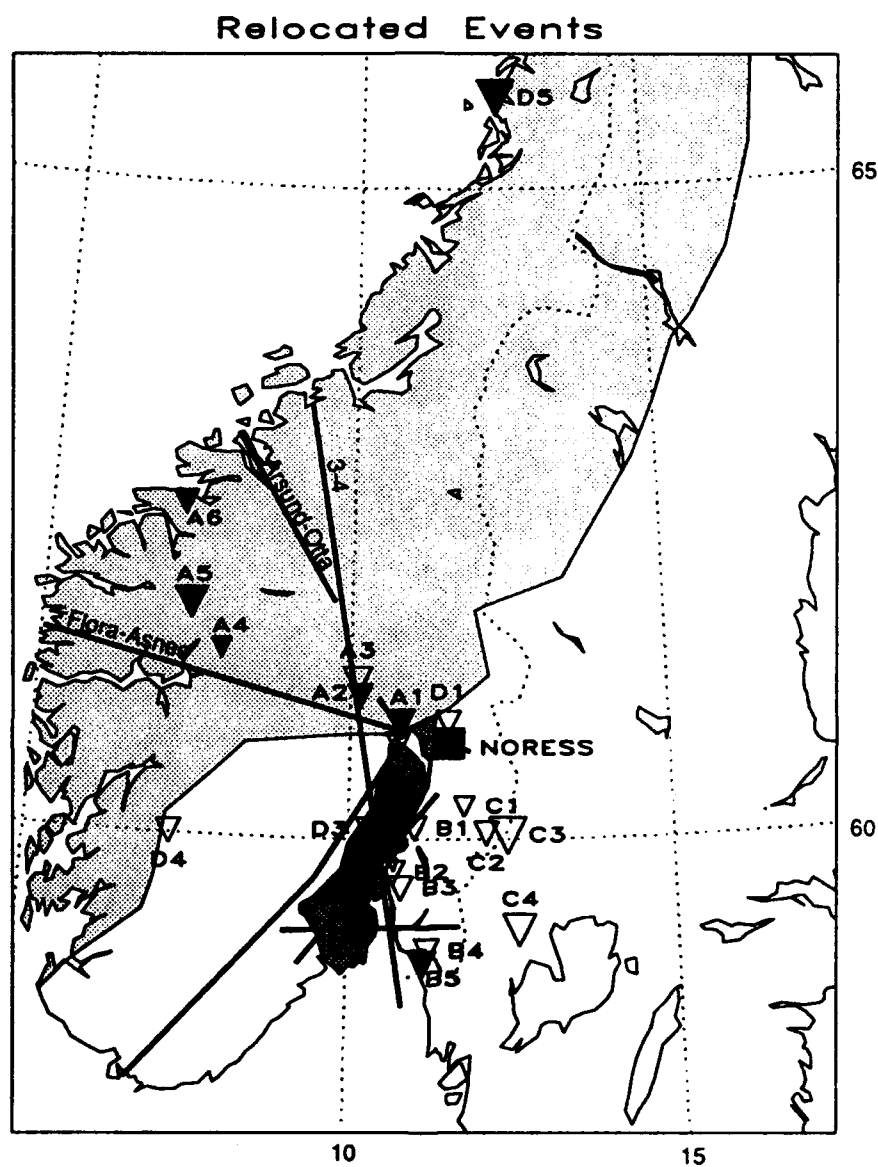


Figure 1. Locations of events recorded at NORESS (triangles). Events presented here are shown by solid triangles. The Caledonian region (light) and the Oslo Graben (dark) are shaded, and locations of refraction profiles are shown by thick lines. Lake Mjøsa is located approximately 30 km SE of NORESS.

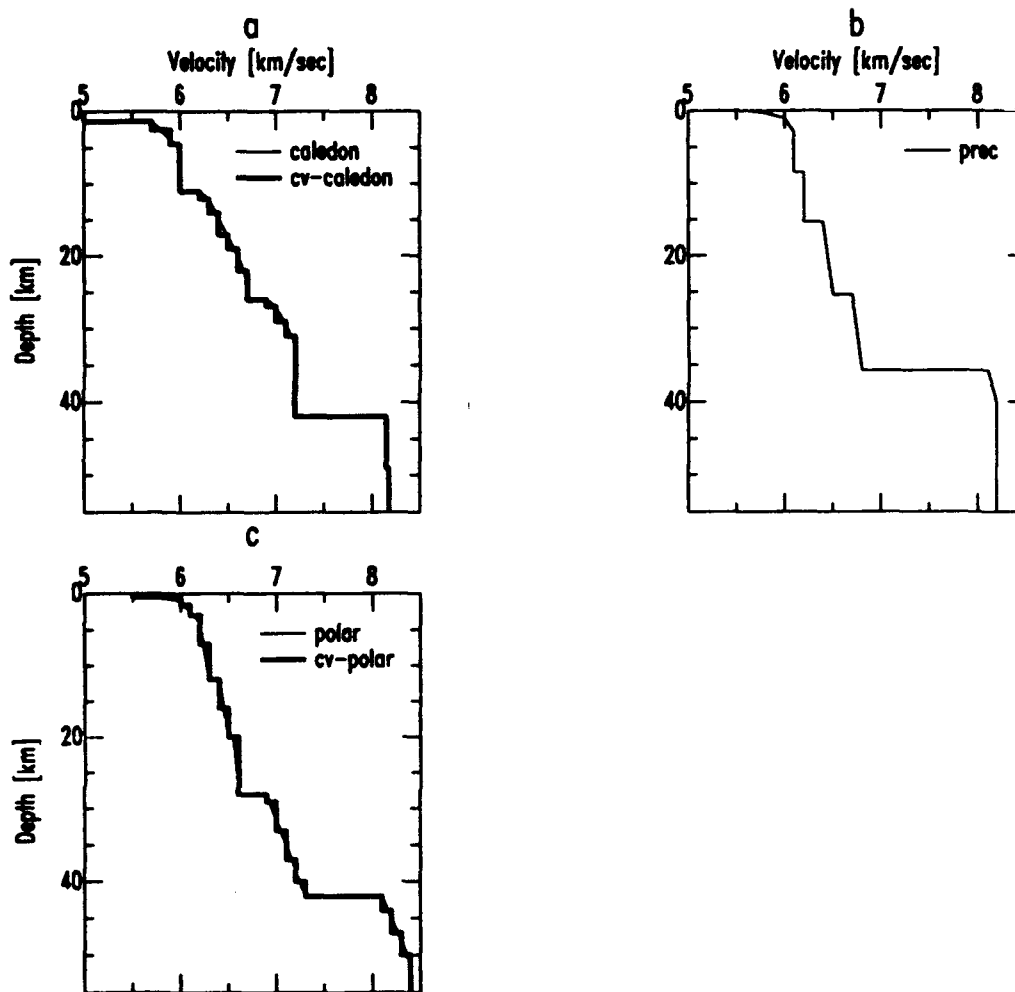
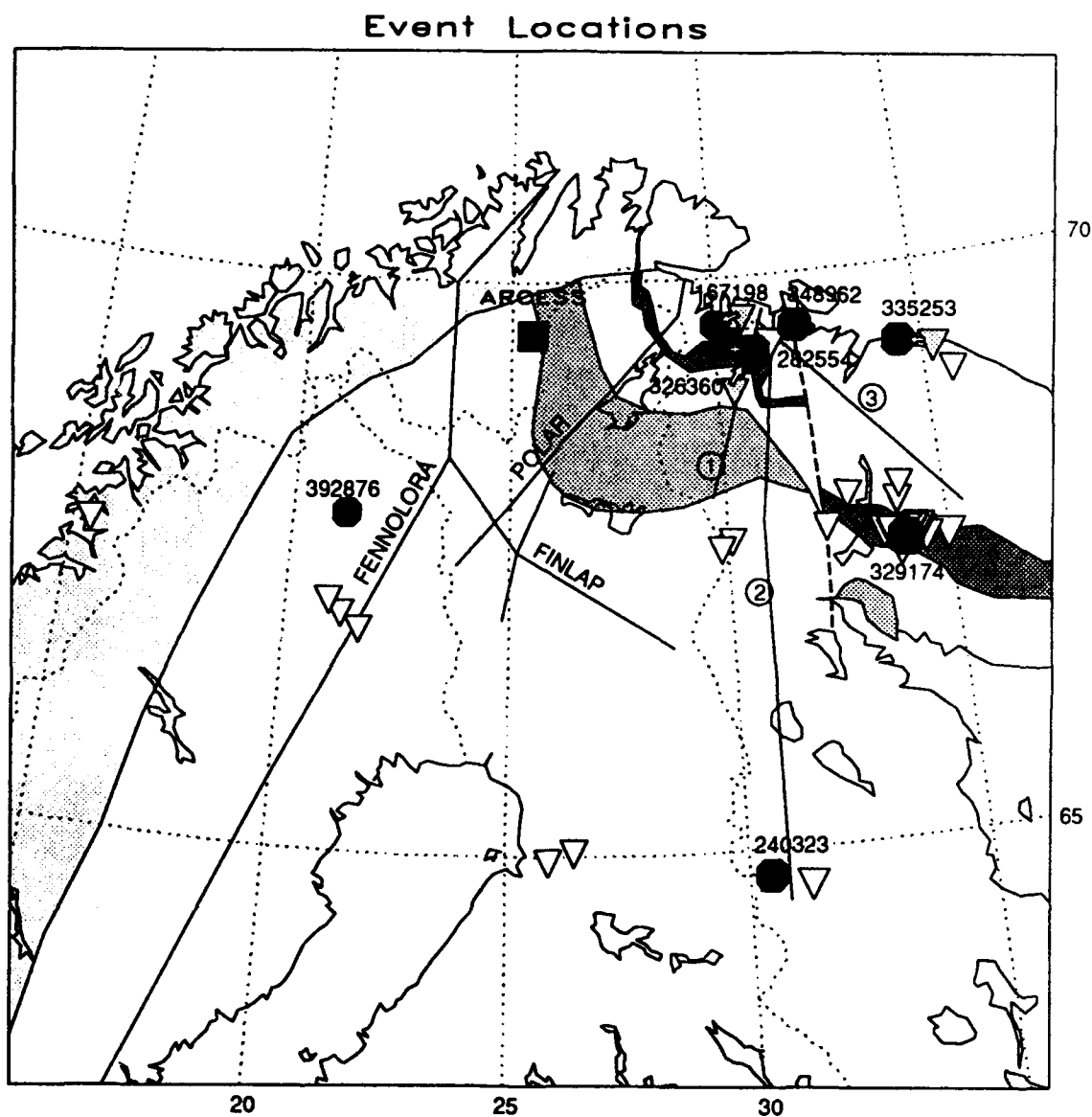


Figure 2. P-wave velocity models: Models used in travel-time and receiver-function analysis (thin lines) and their constant-velocity approximations (thick lines) used in synthetic-seismogram calculations. a) Caledonian model representing average structure in the Caledonides near NORESS; b) Precambrian model representing Precambrian structure around NORESS; c) Polar-profile model representing average structure in the Archaean region around ARCESS.



**Figure 3.** Locations of selected events (triangles) recorded at ARCESS (square). Dashed triangles represent events relocated to the positions indicated by the arrows. Events presented here are shown by solid circles. Refraction profiles are indicated and geologic regions are shaded: Caledonian region (light-grey); Lapland Granulite Belt (grey); Polmak-Pasvik-Pechenga Belt (dark-grey). The cross in the PPP Belt marks the location of the super-deep borehole.

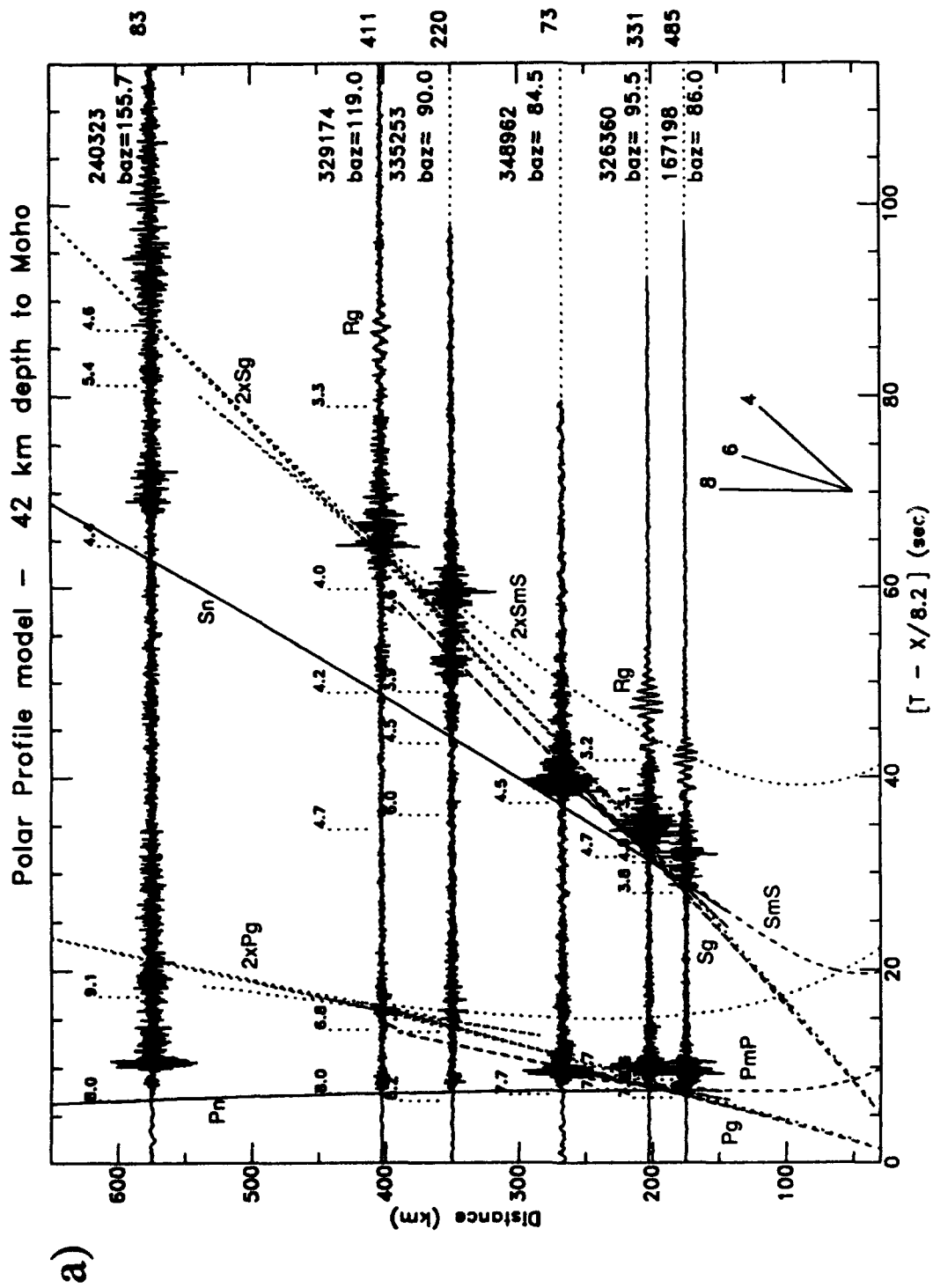


Figure 4a and b. Composite seismograms for the studied events recorded at ARCESS, normalized to maximum amplitude. Stacking velocities used to create beams are indicated above each time section in the seismograms. Travel-time curves of major phases, calculated for the Polar-profile model, are superimposed on the plots. Backazimuth to the event and (Cont.)

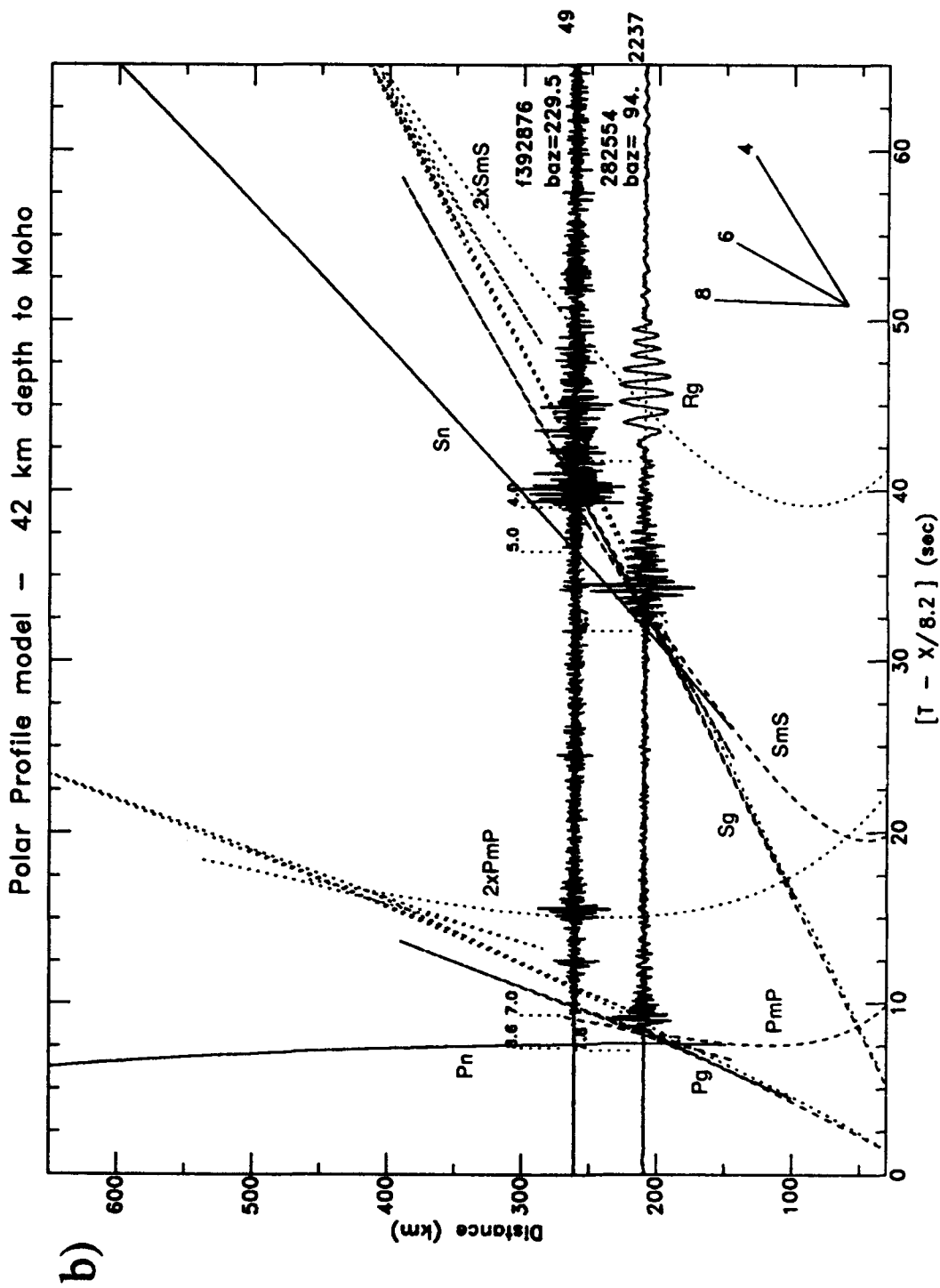


Figure 4 (cont.) maximum amplitude are shown on the right side of each trace. Note the apparent interference in the Rg waves of events 167198 and 326360 (record section a). This is not seen in Rg of event 282554 (record section b), which is much larger and at approximately the same location as event 326360.



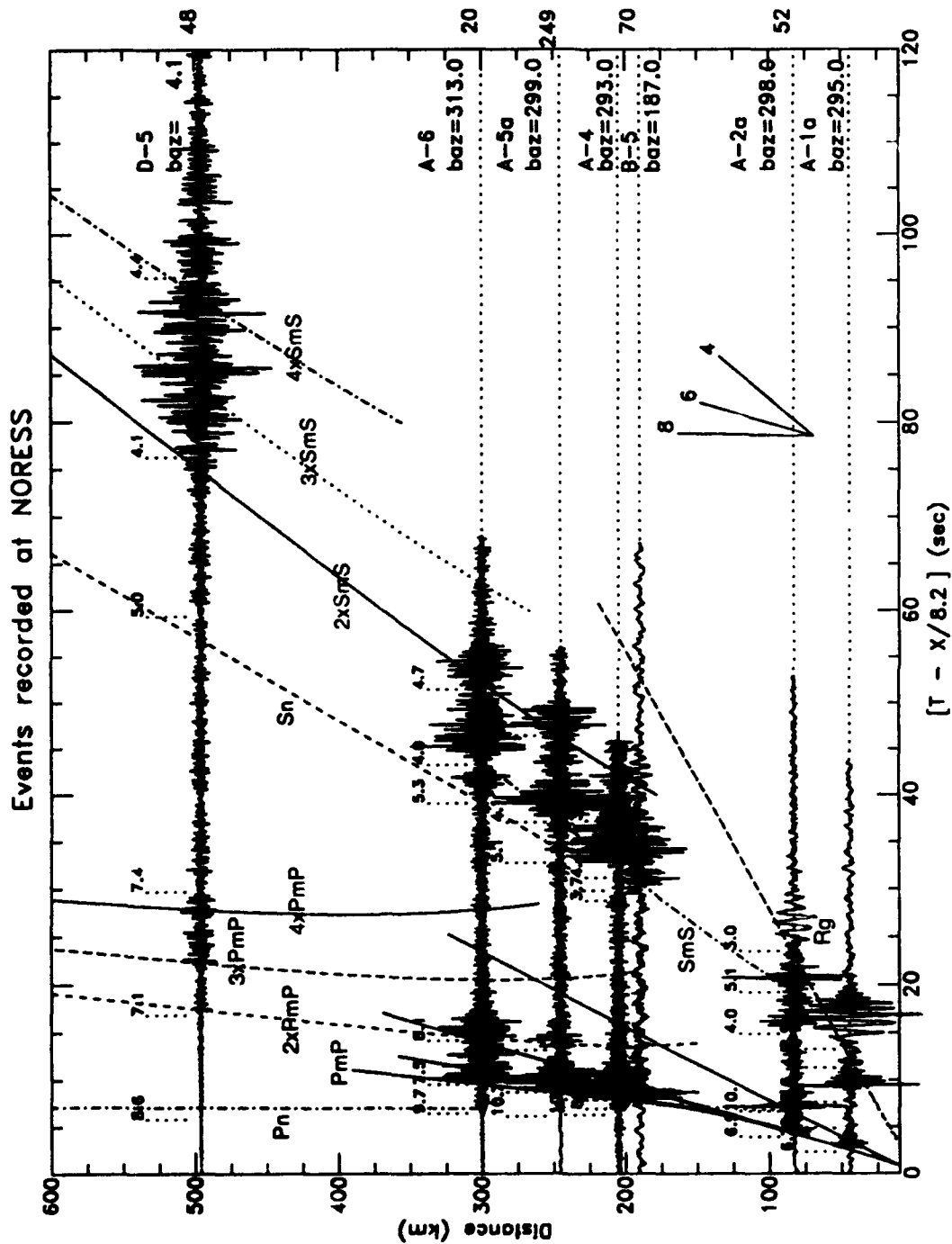


Figure 5. Composite seismograms for events recorded at NORESS. Propagation paths of all events are through the Caledonian region, except for event B-5, which propagates within Precambrian structure. Notice the higher group velocity of the Rg wave from event B-5. Travel-time curves, calculated for a 36 km thick Caledonian model are superimposed on the record section.

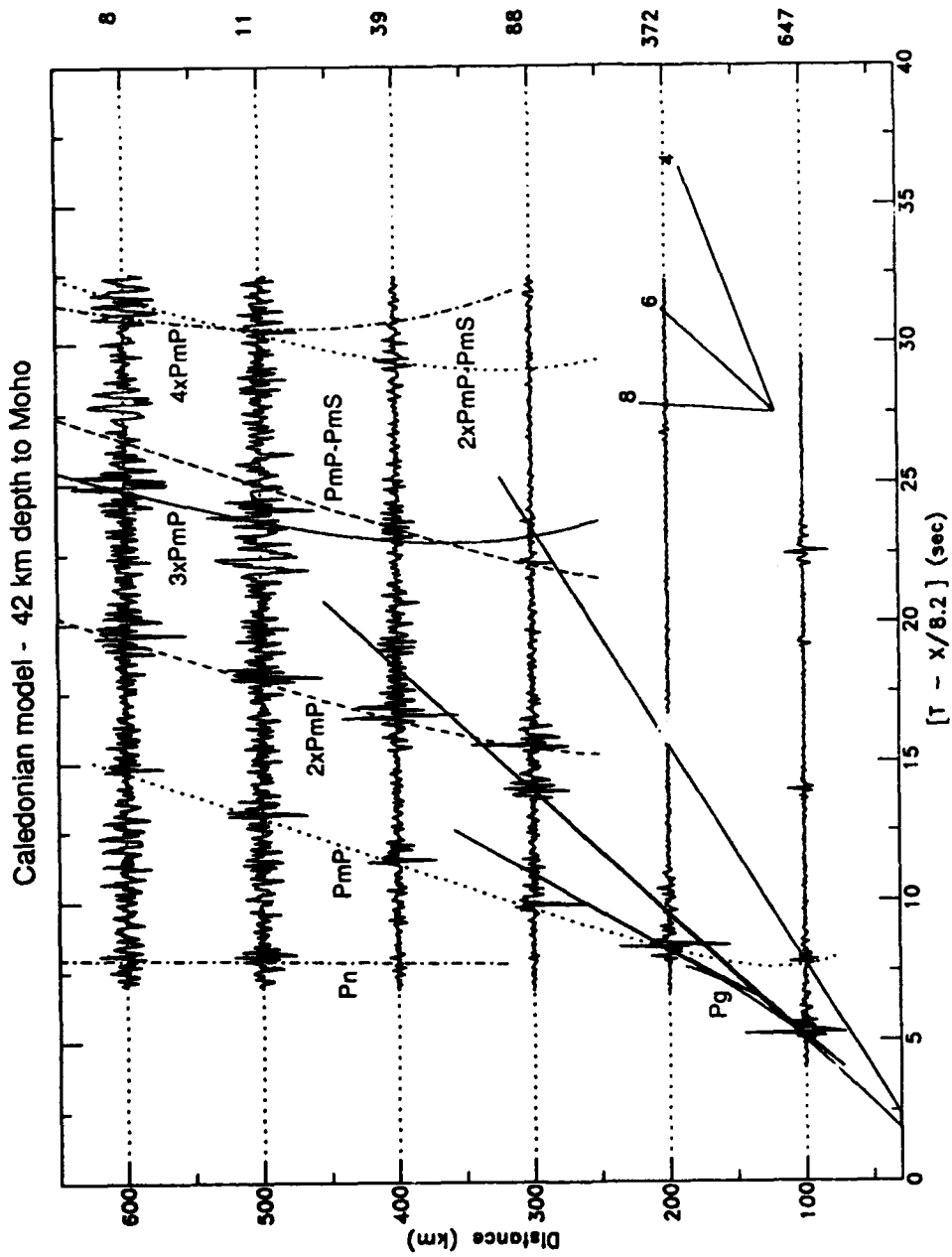


Figure 6. Synthetic P-wave record section for the Polar-profile model, calculated by wavenumber integration. Travel-time curves are superimposed on the plot. The synthetics show similar features as those observed in the composite seismograms.

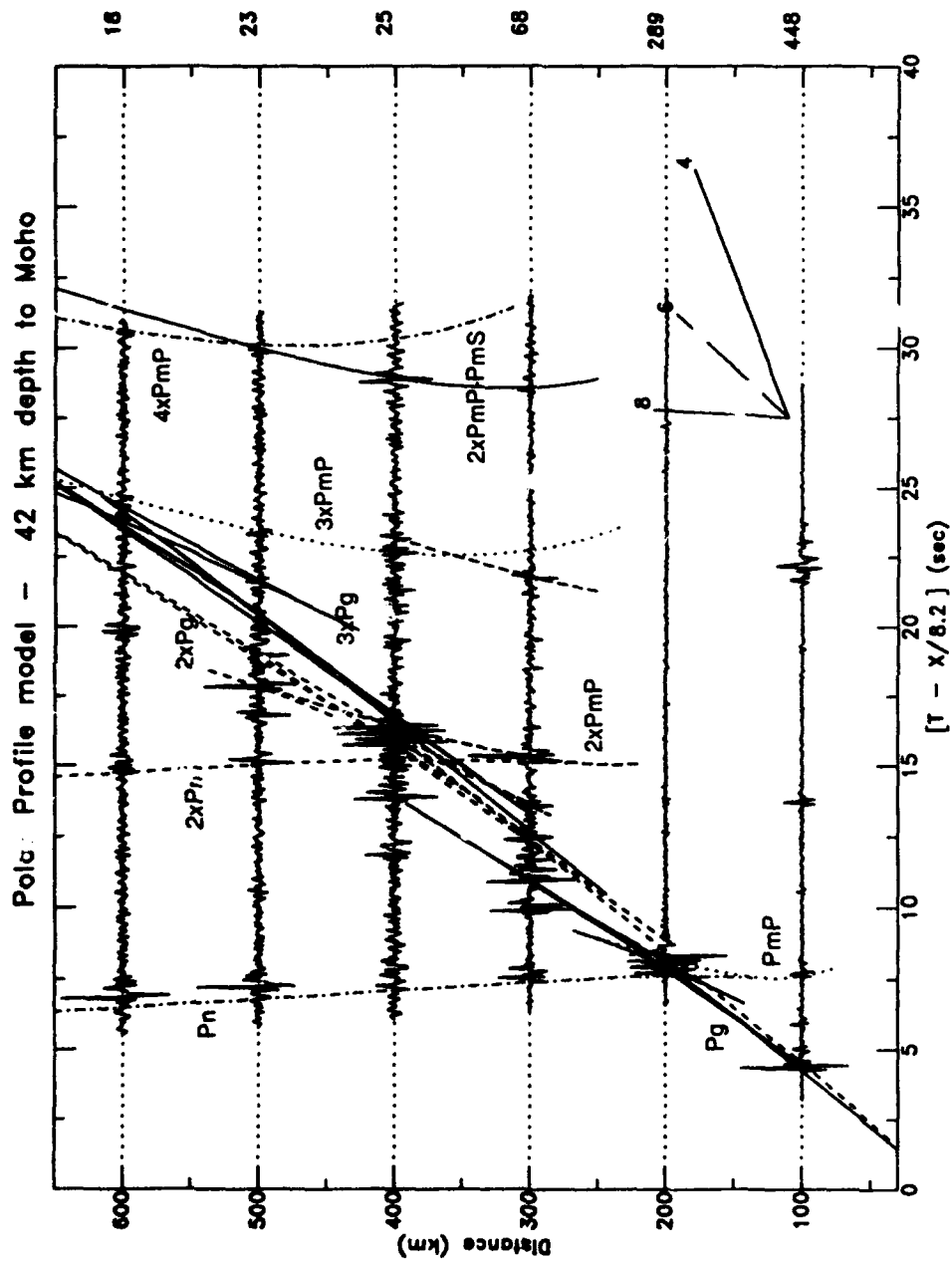


Figure 7. Synthetic P-wave record section for the Caledonian model, calculated by wavenumber integration. Travel-time curves are superimposed on the plot. The record section is significantly different from Figure 6 and has similar characteristics as the NORESS composite record section.

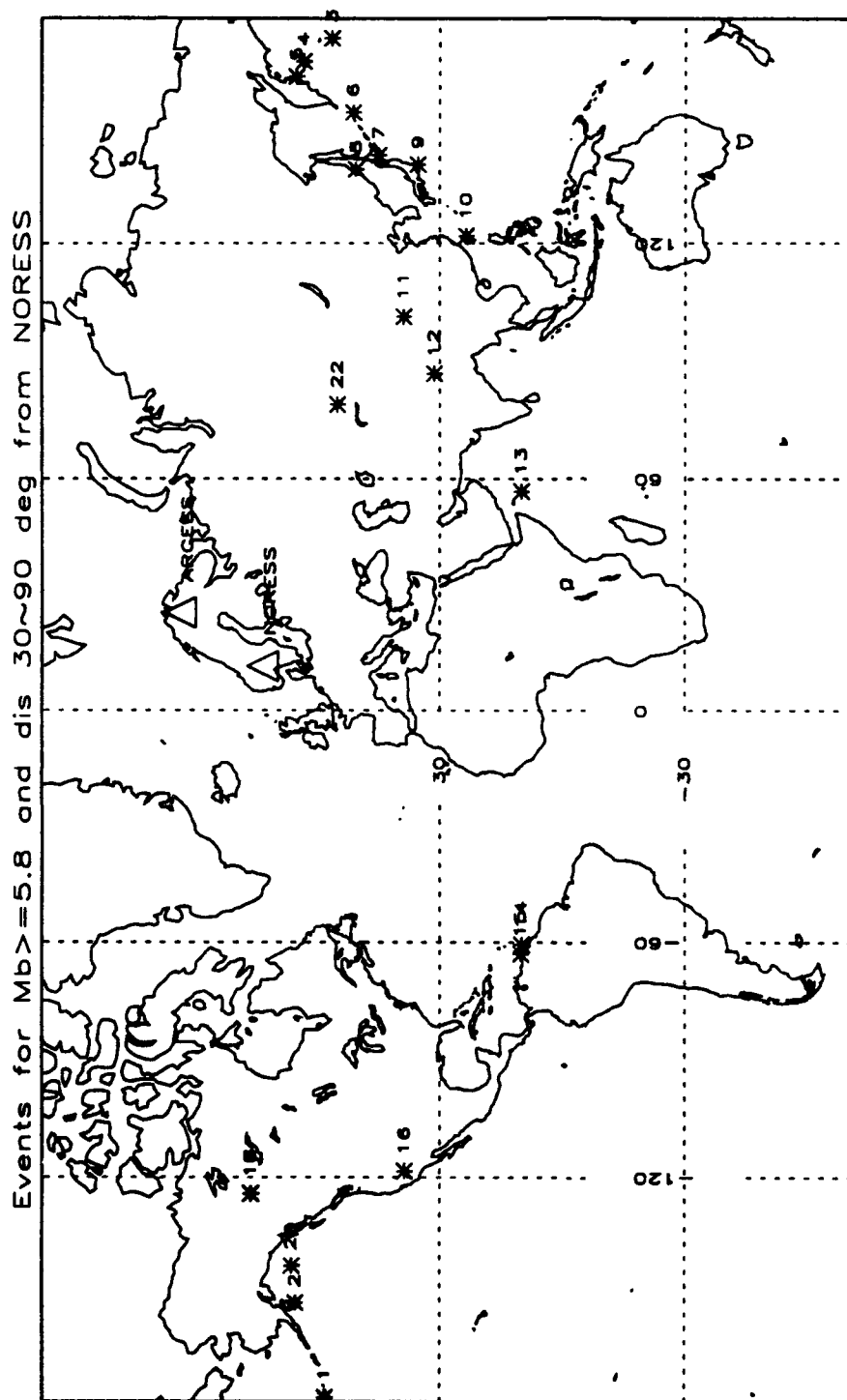
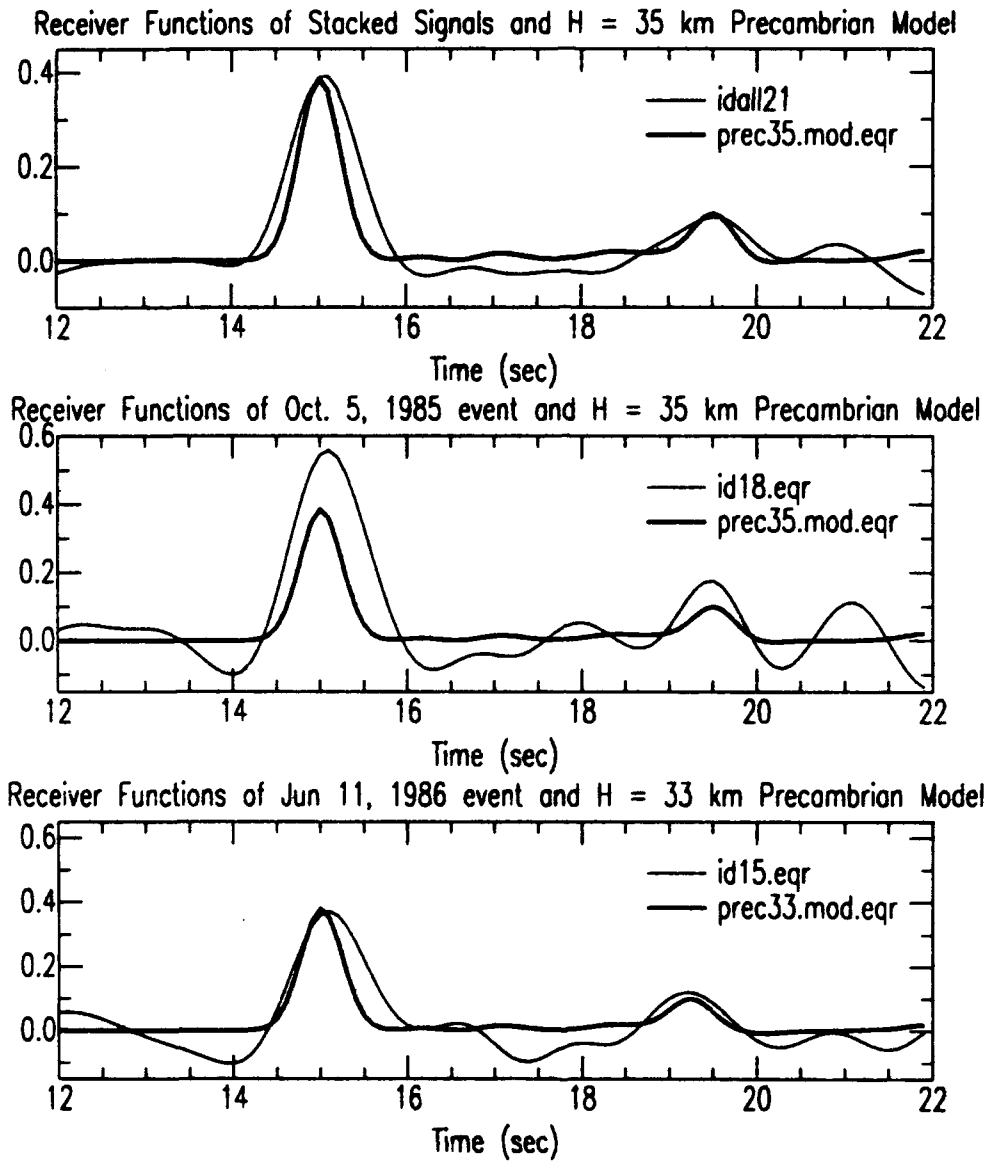


Figure 8. Locations of teleseismic events used in receiver-function calculations.



**Figure 9.** Receiver functions, for data (thin line) and synthetics (thick line). a) Receiver function of stacked data and synthetic receiver function for a 35 km thick Precambrian crust; b) Receiver function for event 18 and the same synthetic as in a; c) Receiver function for event 15 and synthetic receiver function for a 33 km thick Precambrian crust.

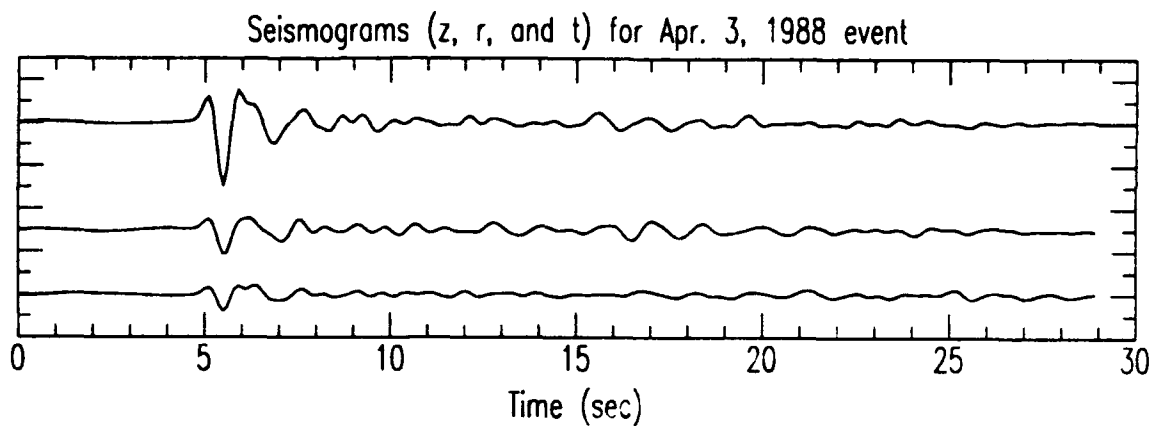


Figure 10 a). Three-component plot (vertical, radial, tangential) of event 22, showing P arrival at 5 sec and a following coda-wave on all components at 15 sec.

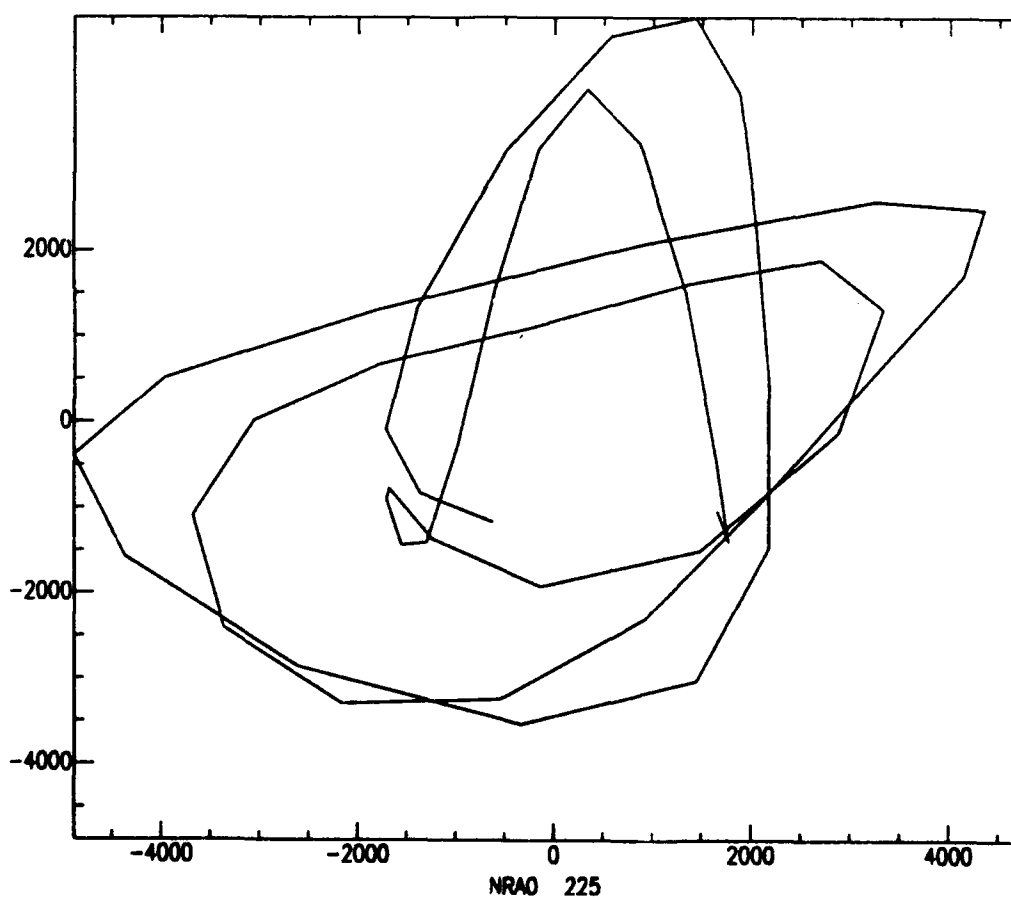


Figure 10 b). Particle motion in the propagation plane between 15 and 20 sec.

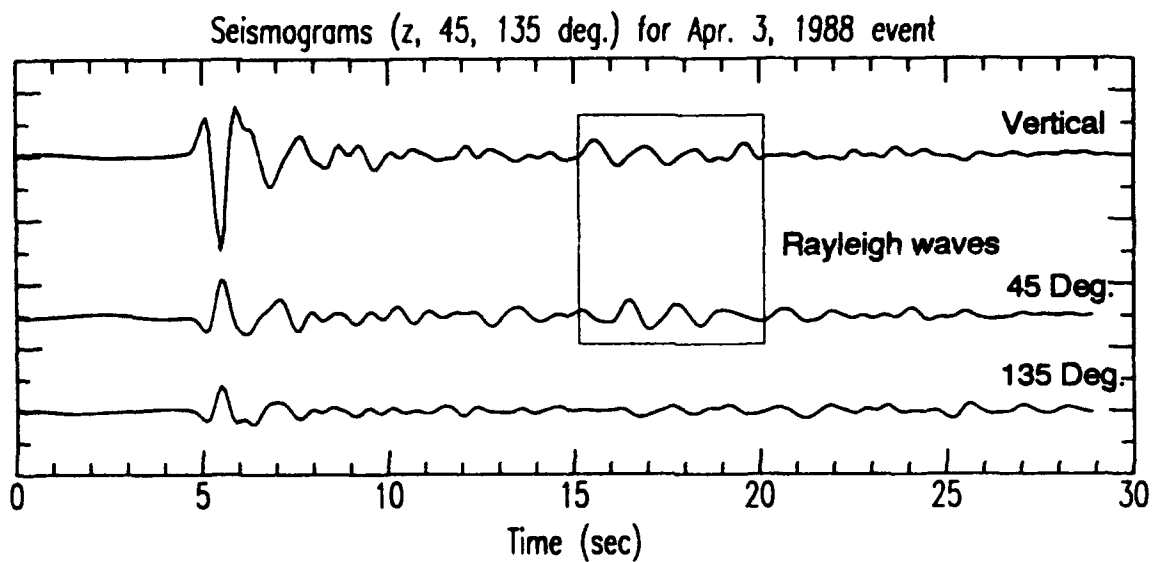


Figure 11 a). Three-component plot of event 22, with horizontal components rotated to 45 and 135 deg.

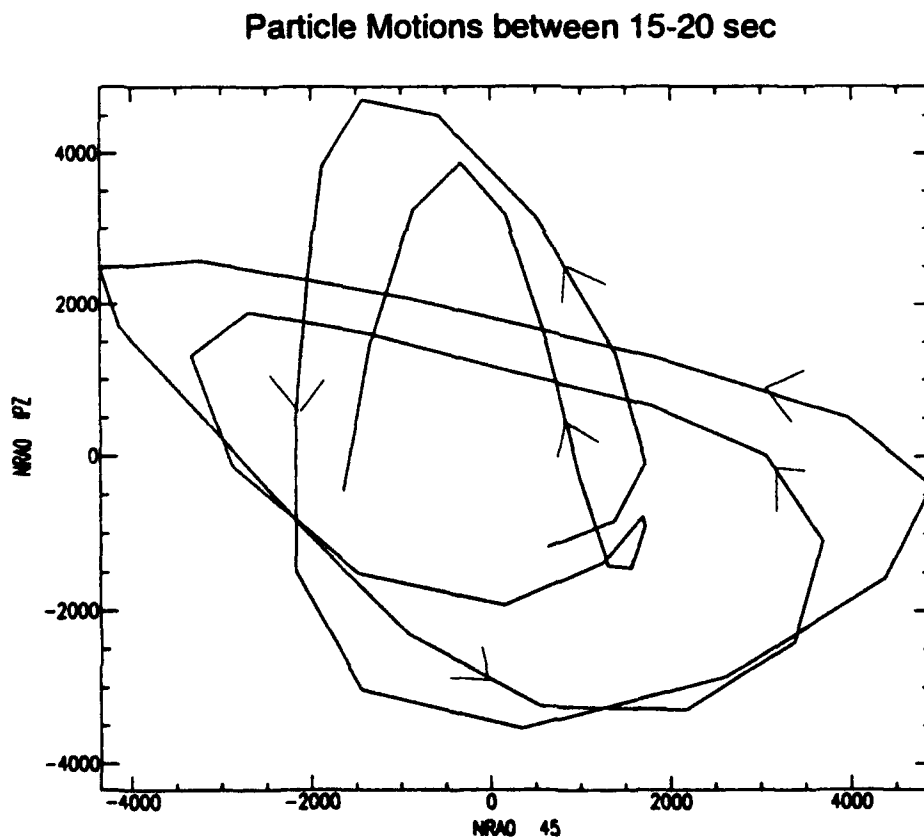


Figure 11 b). Particle motion in the vertical-45 deg. plane, between 15 and 20 sec, showing retrograde elliptical particle motion.

TABLE 1. Event Parameters for NORESS Data

ID	Time		Lat.	Lon.	Depth		Dis.	Back Azi.
	Date	UT	deg	deg	$M_b$	km	deg	deg
1	Mar. 21, 87	10:50: 35.3	52.008	-177.444	6.0	97	67.4	6.0
2	Feb. 18, 87	00:00: 52.6	51.31	-179.31	6.2	33	68.0	7.3
3	Feb. 7, 88	18:15: 05.6	50.785	173.465	6.2	33	67.9	12.3
4	Feb. 29, 88	05:31: 41.4	55.149	167.430	6.1	33	62.9	15.3
5	Dec. 28, 84	10:46: 13.5	56.194	163.460	6.2	33	61.3	17.5
6	May. 16, 86	17:00: 16.7	47.204	154.109	5.8	25	68.2	26.5
7	Jan. 14, 87	11:03: 48.3	42.56	142.88	6.5	99	69.7	36.3
8	May. 7, 87	03:15: 15.5	46.740	139.230	6.0	430	64.8	37.0
9	Jun. 24, 86	02:53: 09.4	34.733	140.502	6.1	48	76.1	41.3
10	Nov. 14, 86	21:20: 4.7	23.963	121.817	6.1	33	78.7	61.1
11	Aug. 26, 86	09:43: 4.2	37.686	101.412	6.1	33	57.9	69.4
12	Jun. 20, 86	17:12: 46.5	31.221	86.862	6.0	33	56.2	85.6
13	Jul. 7, 86	16:26: 56.9	10.421	56.764	6.4	10	60.2	126.4
14	Mar. 10, 88	06:17: 23.3	10.402	-60.587	6.2	56	72.3	259.4
15	Jun. 11, 86	13:48: 03.3	10.602	-62.949	6.0	34	73.2	261.6
16	Jul. 21, 86	14:42: 26.6	37.537	-118.447	6.0	9	73.9	320.7
17	Mar. 25, 88	19:36: 46.4	62.154	-124.182	6.1	10	52.9	335.7
18	Oct. 5, 85	15:31: 21.3	62.237	-124.266	6.5	10	52.8	335.8
19	Dec. 23, 85	05:23: 22.5	62.222	-124.239	6.4	6	52.8	335.8
20	Mar. 6, 88	22:35: 38.1	56.953	-143.032	6.8	10	61.0	344.4
21	Jun. 19, 86	09:09: 12.3	56.418	-152.729	6.0	33	62.5	350.2
22	Apr. 3, 88	01:33: 05.8	49.917	78.945	6.1	0	38.1	75.1



## CONTRACTORS

Prof. Thomas Ahrens  
Seismological Lab, 252-21  
Division of Geological & Planetary Sciences  
California Institute of Technology  
Pasadena, CA 91125

Prof. Keiiti Aki  
Center for Earth Sciences  
University of Southern California  
University Park  
Los Angeles, CA 90089-0741

Prof. Shelton Alexander  
Geosciences Department  
403 Deike Building  
The Pennsylvania State University  
University Park, PA 16802

Dr. Ralph Alewine, III  
DARPA/NMRO  
3701 North Fairfax Drive  
Arlington, VA 22203-1714

Prof. Charles B. Archambeau  
CIRES  
University of Colorado  
Boulder, CO 80309

Dr. Thomas C. Bache, Jr.  
Science Applications Int'l Corp.  
10260 Campus Point Drive  
San Diego, CA 92121 (2 copies)

Prof. Muawia Barazangi  
Institute for the Study of the Continent  
Cornell University  
Ithaca, NY 14853

Dr. Jeff Barker  
Department of Geological Sciences  
State University of New York  
at Binghamton  
Vestal, NY 13901

Dr. Douglas R. Baumgardt  
ENSCO, Inc  
5400 Port Royal Road  
Springfield, VA 22151-2388

Dr. Susan Beck  
Department of Geosciences  
Building #77  
University of Arizona  
Tucson, AZ 85721

Dr. T.J. Bennett  
S-CUBED  
A Division of Maxwell Laboratories  
11800 Sunrise Valley Drive, Suite 1212  
Reston, VA 22091

Dr. Robert Blandford  
AFTAC/TT, Center for Seismic Studies  
1300 North 17th Street  
Suite 1450  
Arlington, VA 22209-2308

Dr. G.A. Bollinger  
Department of Geological Sciences  
Virginia Polytechnical Institute  
21044 Derring Hall  
Blacksburg, VA 24061

Dr. Stephen Bratt  
Center for Seismic Studies  
1300 North 17th Street  
Suite 1450  
Arlington, VA 22209-2308

Dr. Lawrence Burdick  
Woodward-Clyde Consultants  
566 El Dorado Street  
Pasadena, CA 91109-3245

Dr. Robert Burrige  
Schlumberger-Doll Research Center  
Old Quarry Road  
Ridgefield, CT 06877

Dr. Jerry Carter  
Center for Seismic Studies  
1300 North 17th Street  
Suite 1450  
Arlington, VA 22209-2308

Dr. Eric Chael  
Division 9241  
Sandia Laboratory  
Albuquerque, NM 87185

Prof. Vernon F. Cormier  
Department of Geology & Geophysics  
U-45, Room 207  
University of Connecticut  
Storrs, CT 06268

Prof. Steven Day  
Department of Geological Sciences  
San Diego State University  
San Diego, CA 92182

Marvin Denny  
U.S. Department of Energy  
Office of Arms Control  
Washington, DC 20585

Dr. Cliff Frolich  
Institute of Geophysics  
8701 North Mopac  
Austin, TX 78759

Dr. Zoltan Der  
ENSCO, Inc.  
5400 Port Royal Road  
Springfield, VA 22151-2388

Dr. Holly Given  
IGPP, A-025  
Scripps Institute of Oceanography  
University of California, San Diego  
La Jolla, CA 92093

Prof. Adam Dziewonski  
Hoffman Laboratory, Harvard University  
Dept. of Earth Atmos. & Planetary Sciences  
20 Oxford Street  
Cambridge, MA 02138

Dr. Jeffrey W. Given  
SAIC  
10260 Campus Point Drive  
San Diego, CA 92121

Prof. John Ebel  
Department of Geology & Geophysics  
Boston College  
Chestnut Hill, MA 02167

Dr. Dale Glover  
Defense Intelligence Agency  
ATTN: ODT-1B  
Washington, DC 20301

Eric Fielding  
SNEE Hall  
INSTOC  
Cornell University  
Ithaca, NY 14853

Dr. Indra Gupta  
Teledyne Geotech  
314 Montgomery Street  
Alexandria, VA 22314

Dr. Mark D. Fisk  
Mission Research Corporation  
735 State Street  
P.O. Drawer 719  
Santa Barbara, CA 93102

Dan N. Hagedorn  
Pacific Northwest Laboratories  
Battelle Boulevard  
Richland, WA 99352

Prof Stanley Flotte  
Applied Sciences Building  
University of California, Santa Cruz  
Santa Cruz, CA 95064

Dr. James Hannon  
Lawrence Livermore National Laboratory  
P.O. Box 808  
L-205  
Livermore, CA 94550

Dr. John Foley  
NER-Geo Sciences  
1100 Crown Colony Drive  
Quincy, MA 02169

Dr. Roger Hansen  
HQ AFTAC/TTR  
Patrick AFB, FL 32925-6001

Prof. Donald Forsyth  
Department of Geological Sciences  
Brown University  
Providence, RI 02912

Prof. David G. Harkrider  
Seismological Laboratory  
Division of Geological & Planetary Sciences  
California Institute of Technology  
Pasadena, CA 91125

Dr. Art Frankel  
U.S. Geological Survey  
922 National Center  
Reston, VA 22092

Prof. Danny Harvey  
CIRES  
University of Colorado  
Boulder, CO 80309

Prof. Donald V. Helmberger  
Seismological Laboratory  
Division of Geological & Planetary Sciences  
California Institute of Technology  
Pasadena, CA 91125

Prof. Eugene Herrin  
Institute for the Study of Earth and Man  
Geophysical Laboratory  
Southern Methodist University  
Dallas, TX 75275

Prof. Robert B. Herrmann  
Department of Earth & Atmospheric Sciences  
St. Louis University  
St. Louis, MO 63156

Prof. Lane R. Johnson  
Seismographic Station  
University of California  
Berkeley, CA 94720

Prof. Thomas H. Jordan  
Department of Earth, Atmospheric &  
Planetary Sciences  
Massachusetts Institute of Technology  
Cambridge, MA 02139

Prof. Alan Kafka  
Department of Geology & Geophysics  
Boston College  
Chestnut Hill, MA 02167

Robert C. Kemerait  
ENSCO, Inc.  
445 Pineda Court  
Melbourne, FL 32940

Dr. Max Koontz  
U.S. Dept. of Energy/DP 5  
Forrestal Building  
1000 Independence Avenue  
Washington, DC 20585

Dr. Richard LaCoss  
MIT Lincoln Laboratory, M-200B  
P.O. Box 73  
Lexington, MA 02173-0073

Dr. Fred K. Lamb  
University of Illinois at Urbana-Champaign  
Department of Physics  
1110 West Green Street  
Urbana, IL 61801

Prof. Charles A. Langston  
Geosciences Department  
403 Deike Building  
The Pennsylvania State University  
University Park, PA 16802

Jim Lawson, Chief Geophysicist  
Oklahoma Geological Survey  
Oklahoma Geophysical Observatory  
P.O. Box 8  
Leonard, OK 74043-0008

Prof. Thorne Lay  
Institute of Tectonics  
Earth Science Board  
University of California, Santa Cruz  
Santa Cruz, CA 95064

Dr. William Leith  
U.S. Geological Survey  
Mail Stop 928  
Reston, VA 22092

Mr. James F. Lewkowicz  
Phillips Laboratory/GPEH  
Hanscom AFB, MA 01731-5000( 2 copies)

Mr. Alfred Lieberman  
ACDA/VI-OA State Department Building  
Room 5726  
320-21st Street, NW  
Washington, DC 20451

Prof. L. Timothy Long  
School of Geophysical Sciences  
Georgia Institute of Technology  
Atlanta, GA 30332

Dr. Randolph Martin, III  
New England Research, Inc.  
76 Olcott Drive  
White River Junction, VT 05001

Dr. Robert Masse  
Denver Federal Building  
Box 25046, Mail Stop 967  
Denver, CO 80225

Dr. Gary McCartor  
Department of Physics  
Southern Methodist University  
Dallas, TX 75275

Prof. Thomas V. McEvilly  
Seismographic Station  
University of California  
Berkeley, CA 94720

Dr. Art McGarr  
U.S. Geological Survey  
Mail Stop 977  
U.S. Geological Survey  
Menlo Park, CA 94025

Dr. Keith L. McLaughlin  
S-CUBED  
A Division of Maxwell Laboratory  
P.O. Box 1620  
La Jolla, CA 92038-1620

Stephen Miller & Dr. Alexander Florence  
SRI International  
333 Ravenswood Avenue  
Box AF 116  
Menlo Park, CA 94025-3493

Prof. Bernard Minster  
IGPP, A-025  
Scripps Institute of Oceanography  
University of California, San Diego  
La Jolla, CA 92093

Prof. Brian J. Mitchell  
Department of Earth & Atmospheric Sciences  
St. Louis University  
St. Louis, MO 63156

Mr. Jack Murphy  
S-CUBED  
A Division of Maxwell Laboratory  
11800 Sunrise Valley Drive, Suite 1212  
Reston, VA 22091 (2 Copies)

Dr. Keith K. Nakanishi  
Lawrence Livermore National Laboratory  
L-025  
P.O. Box 808  
Livermore, CA 94550

Dr. Carl Newton  
Los Alamos National Laboratory  
P.O. Box 1663  
Mail Stop C335, Group ESS-3  
Los Alamos, NM 87545

Dr. Bao Nguyen  
HQ AFTAC/TTR  
Patrick AFB, FL 32925-6001

Prof. John A. Orcutt  
IGPP, A-025  
Scripps Institute of Oceanography  
University of California, San Diego  
La Jolla, CA 92093

Prof. Jeffrey Park  
Kline Geology Laboratory  
P.O. Box 6666  
New Haven, CT 06511-8130

Dr. Howard Patton  
Lawrence Livermore National Laboratory  
L-025  
P.O. Box 808  
Livermore, CA 94550

Dr. Frank Pilotte  
HQ AFTAC/TT  
Patrick AFB, FL 32925-6001

Dr. Jay J. Pulli  
Radix Systems, Inc.  
2 Taft Court, Suite 203  
Rockville, MD 20850

Dr. Robert Reinke  
ATTN: FCTVTD  
Field Command  
Defense Nuclear Agency  
Kirtland AFB, NM 87115

Prof. Paul G. Richards  
Lamont-Doherty Geological Observatory  
of Columbia University  
Palisades, NY 10964

Mr. Wilmer Rivers  
Teledyne Geotech  
314 Montgomery Street  
Alexandria, VA 22314

Dr. George Rothe  
HQ AFTAC/TTR  
Patrick AFB, FL 32925-6001

Dr. Alan S. Ryall, Jr.  
DARPA/NMRO  
3701 North Fairfax Drive  
Arlington, VA 22209-1714

Dr. Richard Sailor  
TASC, Inc.  
55 Walkers Brook Drive  
Reading, MA 01867

Prof. Charles G. Sammis  
Center for Earth Sciences  
University of Southern California  
University Park  
Los Angeles, CA 90089-0741

Prof. Christopher H. Scholz  
Lamont-Doherty Geological Observatory  
of Columbia University  
Palisades, CA 10964

Dr. Susan Schwartz  
Institute of Tectonics  
1156 High Street  
Santa Cruz, CA 95064

Secretary of the Air Force  
(SAFRD)  
Washington, DC 20330

Office of the Secretary of Defense  
DDR&E  
Washington, DC 20330

Thomas J. Sereno, Jr.  
Science Application Int'l Corp.  
10260 Campus Point Drive  
San Diego, CA 92121

Dr. Michael Shore  
Defense Nuclear Agency/SPSS  
6801 Telegraph Road  
Alexandria, VA 22310

Dr. Matthew Sibol  
Virginia Tech  
Seismological Observatory  
4044 Derring Hall  
Blacksburg, VA 24061-0420

Prof. David G. Simpson  
IRIS, Inc.  
1616 North Fort Myer Drive  
Suite 1440  
Arlington, VA 22209

Donald L. Springer  
Lawrence Livermore National Laboratory  
L-025  
P.O. Box 808  
Livermore, CA 94550

Dr. Jeffrey Stevens  
S-CUBED  
A Division of Maxwell Laboratory  
P.O. Box 1620  
La Jolla, CA 92038-1620

Lt. Col. Jim Stobie  
ATTN: AFOSR/NL  
Bolling AFB  
Washington, DC 20332-6448

Prof. Brian Stump  
Institute for the Study of Earth & Man  
Geophysical Laboratory  
Southern Methodist University  
Dallas, TX 75275

Prof. Jeremiah Sullivan  
University of Illinois at Urbana-Champaign  
Department of Physics  
1110 West Green Street  
Urbana, IL 61801

Prof. L. Sykes  
Lamont-Doherty Geological Observatory  
of Columbia University  
Palisades, NY 10964

Dr. David Taylor  
ENSCO, Inc.  
445 Pineda Court  
Melbourne, FL 32940

Dr. Steven R. Taylor  
Los Alamos National Laboratory  
P.O. Box 1663  
Mail Stop C335  
Los Alamos, NM 87545

Prof. Clifford Thurber  
University of Wisconsin-Madison  
Department of Geology & Geophysics  
1215 West Dayton Street  
Madison, WI 53706

Prof. M. Nafi Toksoz  
Earth Resources Lab  
Massachusetts Institute of Technology  
42 Carleton Street  
Cambridge, MA 02142

Dr. Larry Turnbull  
CIA-OSWR/NED  
Washington, DC 20505

DARPA/RMO/SECURITY OFFICE  
3701 North Fairfax Drive  
Arlington, VA 22203-1714

Dr. Gregory van der Vink  
IRIS, Inc.  
1616 North Fort Myer Drive  
Suite 1440  
Arlington, VA 22209

HQ DNA  
ATTN: Technical Library  
Washington, DC 20305

Dr. Karl Veith  
EG&G  
5211 Auth Road  
Suite 240  
Suitland, MD 20746

Defense Intelligence Agency  
Directorate for Scientific & Technical Intelligence  
ATTN: DTIB  
Washington, DC 20340-6158

Prof. Terry C. Wallace  
Department of Geosciences  
Building #77  
University of Arizona  
Tuscon, AZ 85721

Defense Technical Information Center  
Cameron Station  
Alexandria, VA 22314 (2 Copies)

Dr. Thomas Weaver  
Los Alamos National Laboratory  
P.O. Box 1663  
Mail Stop C335  
Los Alamos, NM 87545

TACTEC  
Battelle Memorial Institute  
505 King Avenue  
Columbus, OH 43201 (Final Report)

Dr. William Wortman  
Mission Research Corporation  
8560 Cinderbed Road  
Suite 700  
Newington, VA 22122

Phillips Laboratory  
ATTN: XPG  
Hanscom AFB, MA 01731-5000

Prof. Francis T. Wu  
Department of Geological Sciences  
State University of New York  
at Binghamton  
Vestal, NY 13901

Phillips Laboratory  
ATTN: GPE  
Hanscom AFB, MA 01731-5000

AFTAC/CA  
(STINFO)  
Patrick AFB, FL 32925-6001

Phillips Laboratory  
ATTN: TSML  
Hanscom AFB, MA 01731-5000

DARPA/PM  
3701 North Fairfax Drive  
Arlington, VA 22203-1714

Phillips Laboratory  
ATTN: SUL  
Kirtland, NM 87117 (2 copies)

DARPA/RMO/RETRIEVAL  
3701 North Fairfax Drive  
Arlington, VA 22203-1714

Dr. Michel Bouchon  
I.R.I.G.M.-B.P. 68  
38402 St. Martin D'Heres  
Cedex, FRANCE

Dr. Michel Campillo  
Observatoire de Grenoble  
I.R.I.G.M.-B.P. 53  
38041 Grenoble, FRANCE

Dr. Jorg Schlittenhardt  
Federal Institute for Geosciences & at'l Res.  
Postfach 510153  
D-3000 Hannover 51, GERMANY

Dr. Kin Yip Chun  
Geophysics Division  
Physics Department  
University of Toronto  
Ontario, CANADA

Dr. Johannes Schweitzer  
Institute of Geophysics  
Ruhr University/Bochum  
P.O. Box 1102148  
4360 Bochum 1, GERMANY

Prof. Hans-Peter Harjes  
Institute for Geophysic  
Ruhr University/Bochum  
P.O. Box 102148  
4630 Bochum 1, GERMANY

Prof. Eystein Husebye  
NTNF/NORSAR  
P.O. Box 51  
N-2007 Kjeller, NORWAY

David Jepsen  
Acting Head, Nuclear Monitoring Section  
Bureau of Mineral Resources  
Geology and Geophysics  
G.P.O. Box 378, Canberra, AUSTRALIA

Ms. Eva Johannisson  
Senior Research Officer  
National Defense Research Inst.  
P.O. Box 27322  
S-102 54 Stockholm, SWEDEN

Dr. Peter Marshall  
Procurement Executive  
Ministry of Defense  
Blacknest, Brimpton  
Reading FG7-FRS, UNITED KINGDOM

Dr. Bernard Massinon, Dr. Pierre Mechler  
Societe Radiomana  
27 rue Claude Bernard  
75005 Paris, FRANCE (2 Copies)

Dr. Svein Mykkeltveit  
NTNF/NORSAR  
P.O. Box 51  
N-2007 Kjeller, NORWAY (3 Copies)

Prof. Keith Priestley  
University of Cambridge  
Bullard Labs, Dept. of Earth Sciences  
Madingley Rise, Madingley Road  
Cambridge CB3 0EZ, ENGLAND